PHYSICAL REVIEW FLUIDS **1**, 042401(R) (2016)

Two regimes of flux scaling in axially homogeneous turbulent convection in vertical tube

Shashikant S. Pawar and Jaywant H. Arakeri*

Department of Mechanical Engineering, Indian Institute of Science, Bangalore 560012, India

(Received 19 January 2016; published 15 August 2016)

From experiments of axially homogeneous turbulent convection in a vertical tube using heat (Prandtl number $\mathrm{Pr} \simeq 6$) and brine ($\mathrm{Pr} \simeq 600$) we show that at sufficiently high Rayleigh numbers (Ra_g), the Nusselt number $\mathrm{Nu}_g \sim (\mathrm{Ra}_g\mathrm{Pr})^{1/2}$, which corresponds to the so-called ultimate regime scaling. In heat experiments below certain Ra_g, however, there is transition to a new regime, $\mathrm{Nu}_g \sim (\mathrm{Ra}_g\mathrm{Pr})^{0.3}$. This transition also seems to exist in earlier reported data for $\mathrm{Pr} = 1$ and $\mathrm{Pr} \simeq 600$, at different Ra_g. However, the transition occurs at a single Grashof number, $\mathrm{Gr}_{gc} \simeq 1.6 \times 10^5$, and unified flux scalings for $\mathrm{Pr} \geqslant 1$, $\mathrm{Nu}_g/\mathrm{Pr} \sim \mathrm{Gr}_g^{0.3}$, and $\mathrm{Nu}_g/\mathrm{Pr} \sim \mathrm{Gr}_g^{1/2}$ can be given for the two regimes.

DOI: 10.1103/PhysRevFluids.1.042401

Natural turbulent convection studies are important in understanding many natural phenomena, as also in the design of engineering systems. Turbulent Rayleigh-Bénard convection (RBC) has been a prototype problem in these studies. The dependence of heat transport on thermal forcing in turbulent convection is dictated by a scaling law usually expressed as $\mathrm{Nu} \sim \mathrm{Ra}^n\mathrm{Pr}^m$, where $\mathrm{Nu} = \frac{\dot{q}}{k\frac{\Delta T}{L}}$, $\mathrm{Ra} = \frac{\beta g \Delta T L^3}{\nu\alpha}$, and $\mathrm{Pr} = \frac{\nu}{\alpha}$ are the Nusselt, Rayleigh, and Prandtl numbers, respectively, and n and m are the scaling exponents. $\dot{q}$ is the heat flux, ΔT and L are respectively the temperature difference and the distance between the horizontal plates, g is the gravitational constant, and β, k, ν, and α are respectively cubic expansion coefficient, thermal conductivity, kinematic viscosity, and thermal diffusivity of the working fluid. For convection driven by concentration difference, we use the same notation with the understanding that Pr represents the Schmidt number, $\mathrm{Sc} = \frac{\nu}{D}$, where D is diffusivity of salt and the other material properties are suitably changed. For a large range of Ra, the scaling exponent n obtained in most of the experimental investigations is close to 0.3 [1]. Boundary layer dynamics and the associated plumes essentially determine the flux and explains its weak dependence on L implied by $n \simeq 0.3$ [2,3]. In a theoretical work, Kraichnan [4] proposed different regimes of heat flux scaling in turbulent thermal convection. The regime of very high Ra and $\mathrm{Pr} < 0.15$, in which he obtained the asymptotic scaling, $\mathrm{Nu} \sim (\mathrm{RaPr})^{\frac{1}{2}}(\ln \mathrm{Ra})^{-\frac{3}{2}}$, was later called the ultimate regime in turbulent convection. The scaling $\mathrm{Nu} \sim (\mathrm{RaPr})^{\frac{1}{2}}$ was also proposed by Spiegel [5], in stellar convection for $\mathrm{Pr} \ll 1$. Except the logarithmic correction in the former, the two scalings are similar and imply that the flux is independent of kinematic viscosity and thermal diffusivity. A unifying theory proposed by Grossmann and Lohse [6] also reiterates Kraichnan's prediction of $\mathrm{Nu} \sim \mathrm{Ra}^{\frac{1}{2}}\mathrm{Pr}^{\frac{1}{2}}$ for one of the regimes in Ra-Pr phase space (roughly $10^{11} < \mathrm{Ra} < 3 \times 10^{14}$ and $0.006 < \mathrm{Pr} < 1.4$). Although Ra as high as 10^{17} has been achieved [7], whether the $\frac{1}{2}$ power law scaling exists in RBC has still not been satisfactorily resolved [8–10]. By extending the unifying theory to $\mathrm{Ra} > 10^{11}$ Grossmann and Lohse [11] show, however, that the scaling exponent n is effectively 0.35–0.42 in the ultimate regime when the logarithmic correction due to turbulent boundary layer is considered. The theory supports the scaling exponent of 0.38 observed by He *et al.* [9] in their experiments for $\mathrm{Ra} > 10^{14}$. Logarithmic correction in the flux scaling proposed by Kraichnan has also been used earlier [8,12] in the interpretation of the observed scaling exponent, $1/3 < n < 1/2$.

*jaywant@mecheng.iisc.ernet.in

Another type of turbulent convective flow where the $(\mathrm{RaPr})^{\frac{1}{2}}$ scaling (ultimate regime) is relatively easily achieved is that created in a long vertical tube *open at both ends* [13–18]. The top and bottom boundary layers are thus absent. There are several features that make tube convection different from RBC and interesting. A *linear mean density gradient* exists in the middle portion of the tube away from the ends [14], where the flow is axially homogeneous. Earlier [15] and present measurements show that the time-averaged velocities are zero and the flow is axisymmetric. Since the mean shear and the Reynolds shear stresses are also zero, the turbulent production is solely due to buoyancy. Moreover, the fluxes and Reynolds numbers obtained in tube convection are orders of magnitude higher than those in RBC at similar Rayleigh numbers. The Rayleigh number is defined based on the linear mean density gradient in the homogeneous region,

$$\mathrm{Ra}_g = \frac{g}{\rho_0}\frac{\left(\frac{d\bar{\rho}}{dz}\right)d^4}{\nu\alpha}, \tag{1}$$

where d is the tube diameter. The subscript g is used to distinguish the gradient-based nondimensional numbers of the present case from those in Rayleigh-Bénard convection. Arakeri *et al.* [13] identified different flow types as the Rayleigh number was varied for $\mathrm{Pr} \simeq 600$: laminar half-and-half flow, onset of helical instability, unsteady laminar flow, and fully turbulent flow. For the fully turbulent case, they proposed the scales for density and vertical velocity fluctuations from a mixing length model [13],

$$\rho' \sim \left(\frac{d\bar{\rho}}{dz}\right)d \qquad \text{and} \qquad w' \sim \sqrt{\frac{g}{\rho_0}\left(\frac{d\bar{\rho}}{dz}\right)d^2} = w_m. \tag{2}$$

Nusselt and Reynolds number scalings then become [14]

$$\mathrm{Nu}_g \sim \mathrm{Ra}_g^{\frac{1}{2}}\mathrm{Pr}^{\frac{1}{2}} \qquad \text{and} \qquad \mathrm{Re} \sim \mathrm{Ra}_g^{\frac{1}{2}}\mathrm{Pr}^{-\frac{1}{2}}, \tag{3}$$

respectively. The Reynolds number scaling can also be written as $\mathrm{Re} \sim \mathrm{Gr}_g^{\frac{1}{2}}$, where $\mathrm{Gr}_g = \frac{g}{\rho_0}\frac{\frac{d\bar{\rho}}{dz}d^4}{\nu^2}$ is the gradient Grashof number. These scalings were confirmed by the experiments using brine and fresh water to create the density difference [15] and in direct numerical simulations (DNS) by Schmidt *et al.* [18] for $\mathrm{Pr} = 1$. The highest value of Ra_g in the experiments was about 10^8 and Pr was about 600. It may be mentioned that earlier similar scalings were also obtained in three-dimensional periodic box simulations by Lohse and Toschi [19] and using a shell model by Ching and Ko [20]. The similarity of flux scaling obtained in three-dimensional periodic box [19] and in cylindrical cell geometry [15,18] indicates the passive role of side walls in the flux transport. Gibert *et al.* [17] have used a square-cross-sectional channel with height-to-width ratio of 2 in their experiments; using the ratio of rms temperature fluctuations to the mean temperature gradient as the length scale for Ra, they get $\mathrm{Nu} \sim (\mathrm{RaPr})^{\frac{1}{2}}$. Subsequently [21], using particle image velocimetry (PIV), the time-averaged flow was found to be half-and-half type with random flow reversals.

In this paper we present the results obtained from the measurements of flux carried out in two sets of axially homogeneous tube convection experiments. In one, the density difference was created using brine, and in the other, it was created using heat. For the experiments using brine, Reynolds number scaling is also presented, which is obtained from the velocity measurements using PIV. Figure 1 shows schematically the experimental setup. A long vertical tube (length-to-diameter ratio $L/d = 10$) interconnects two tanks; $L/d = 10$ was chosen to obtain axially homogeneous conditions over several diameter lengths [15]. The convection is driven by the unstable density difference created across the tube ends and is turbulent for the range of Rayleigh numbers being investigated.

In the experiments using brine ($\mathrm{Pr} \simeq 600$), the tube diameter was 140 mm, L/d was 10, and the range of Rayleigh numbers was $3 \times 10^8 < \mathrm{Ra}_g < 8 \times 10^9$, two orders of magnitude larger than those reported by Cholemari and Arakeri [15]. The density difference between the two tanks at the beginning of each experiment, $\frac{\Delta\rho}{\rho_0}$, was about 0.007. These were run-down experiments lasting for

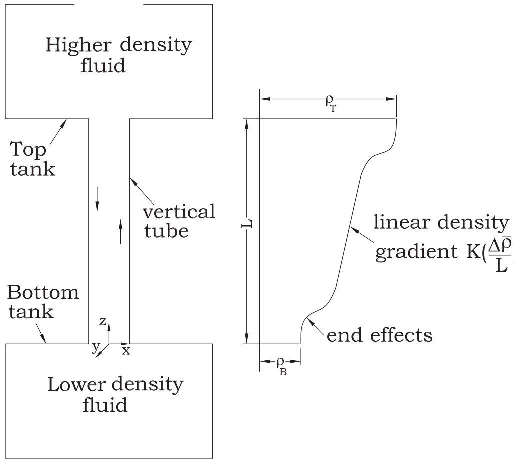

FIG. 1. Schematic of the experimental setup.

about 6 h. For sufficiently small time periods, the flow can thus be considered as quasisteady. The experimental procedure can be found in the earlier work [13–15]. Instantaneous salt concentration C in each tank was measured using conductivity probes. The average salt flux was calculated from the measured concentration as $\langle F\rangle = \frac{V}{A}\frac{dC}{dt}$, where V and A are the volumes of the tank and the cross-sectional area of the tube respectively.

Two types of setup were used in the heat experiments. In the first type, setup A, chilled water from a constant temperature bath was circulated in the top tank while an immersion heater was used to heat the fluid in the bottom tank. The tanks and the tube were insulated with nitrile rubber insulation. A guard heater on the bottom tank compensated for the heat loss to the surroundings. The heat flux in the tube was calculated from the immersion heater input power. Temperatures measured by T-type thermocouples along the length of the tube showed a linear mean temperature gradient $\frac{d\overline{T}}{dz}$, over the tube length, except near the ends. The tube diameters used were 15.5, 31.5, and 50 mm with $L/d = 10$, which covered the range $5 \times 10^4 < \mathrm{Ra}_g < 5 \times 10^6$. Experiments carried out in setup A were repeated in setup B, which had no visualization window and had tanks about 10 times smaller in volume than those in setup A. Results from both the setups were in good agreement, indicating that the results were not affected by heat loss to the surroundings.

Figure 2 shows the variation of Nu_g with $\mathrm{Ra}_g\mathrm{Pr}$ for the brine experiments. The measurements are shown by the filled circles. The power law fit, $(0.77 \pm 0.1)(\mathrm{Ra}_g\mathrm{Pr})^{\frac{1}{2}}$, is shown by a dashed line, which is as per the scaling predicted by the mixing length model [Eq. (3)]. Figure 3 shows variation of Reynolds number $\mathrm{Re} = \frac{\langle w_{\mathrm{rms}}\rangle d}{\nu}$, defined based on the average rms value of vertical velocity and tube diameter, with $\mathrm{Ra}_g/\mathrm{Pr}$; data are from the current measurements and those in the lower Rayleigh number range are from Cholemari and Arakeri [15]. The velocity fields are obtained from PIV measurements carried out in the longitudinal plane passing through the tube axis in the middle portion of the tube, where the flow is axially homogeneous. The measurements are shown by filled circles and the power law fit $(0.79 \pm 0.02)\mathrm{Ra}_g^{\frac{1}{2}}\mathrm{Pr}^{-\frac{1}{2}}$ is shown by a dashed line, which again follows the mixing length model prediction [Eq. (3)]. Profiles of the vertical rms velocity normalized by the value averaged over the cross section, for two Rayleigh numbers are shown in Fig. 3(a). The rms velocity gradually increases from the tube axis, up to a certain x/d location marked by a dashed line, beyond which a steep decrease can be noticed due to the viscous damping in the near wall region. Even though the rms value averaged over the cross section shows the same scaling over the range of Ra_g values covered, the profiles do show some Rayleigh number dependence: The location

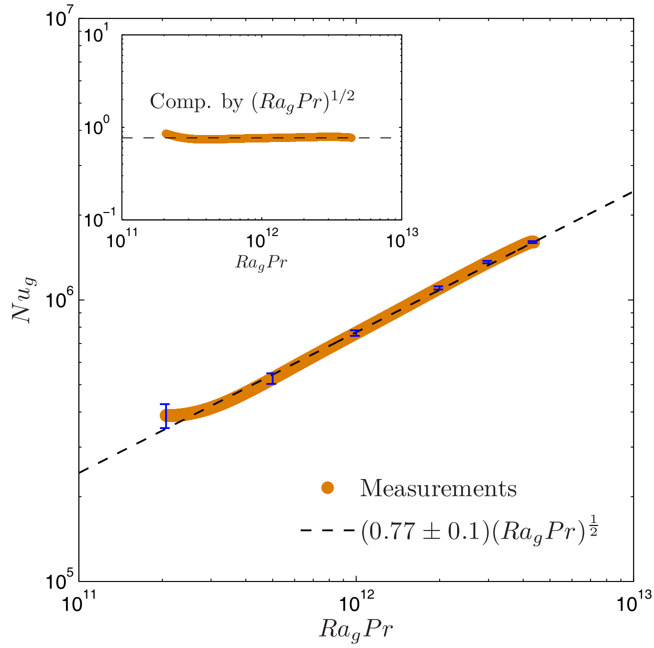

FIG. 2. Nu_g vs $\mathrm{Ra}_g\mathrm{Pr}$ obtained from the measurements in the present experiments using brine. Compensated data are shown in the inset.

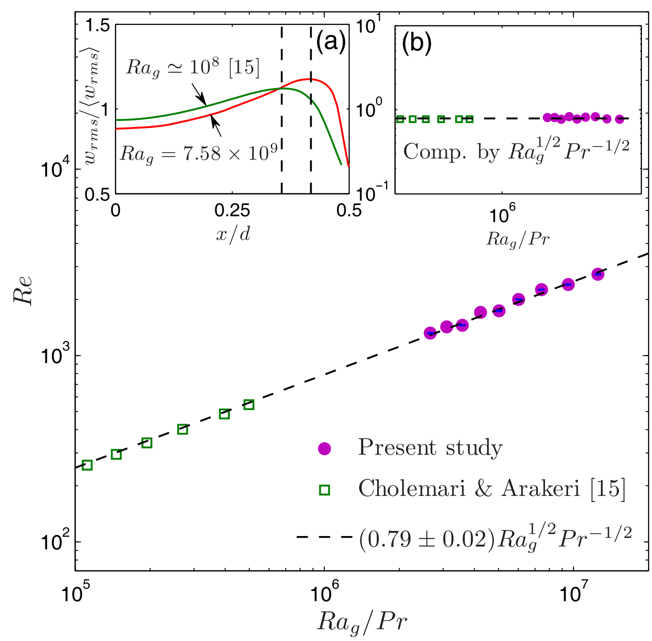

FIG. 3. Re vs $\mathrm{Ra}_g/\mathrm{Pr}$ obtained from the present measurements in brine experiments are shown by filled circles (magenta online), and hollow squares (green online) are from Cholemari and Arakeri [15]. Profiles of vertical rms velocity for two Rayleigh numbers are shown in inset (a); inset (b) shows the compensated data.

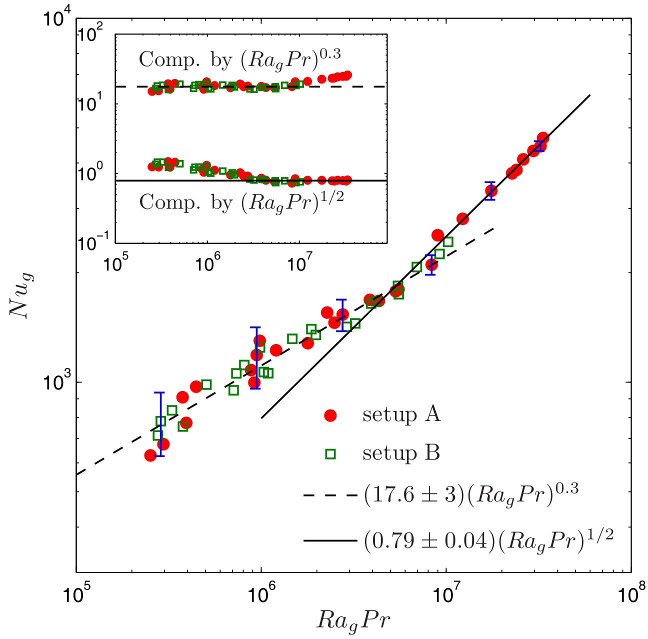

FIG. 4. Nu_g vs $\mathrm{Ra}_g\mathrm{Pr}$ obtained from the measurements in experiments using heat. Data compensated by $(\mathrm{Ra}_g\mathrm{Pr})^{0.3}$ and $(\mathrm{Ra}_g\mathrm{Pr})^{1/2}$ are shown in the inset.

of maximum value shifts towards the wall with increasing Rayleigh number. This point is further discussed below.

Figure 4 shows the variation of Nu_g with $\mathrm{Ra}_g\mathrm{Pr}$ for the heat experiments. The scaling $\mathrm{Nu}_g = (0.79 \pm 0.04)(\mathrm{Ra}_g\mathrm{Pr})^{\frac{1}{2}}$, shown by a continuous line, is observed for $\mathrm{Ra}_g\mathrm{Pr} > 5.6 \times 10^6$, which is again as per the flux scaling obtained from the mixing length model. For $\mathrm{Ra}_g\mathrm{Pr} < 5.6 \times 10^6$, however, we observe a different scaling, $\mathrm{Nu}_g = (17.6 \pm 3)(\mathrm{Ra}_g\mathrm{Pr})^{0.3}$.

Results from different studies in turbulent convection in a vertical tube are combined in Fig. 5. These include results of the present study from experiments using brine ($\mathrm{Pr} \simeq 600$) and heat ($\mathrm{Pr} \simeq 6$) as well as results from the previous work by Tovar [16] ($\mathrm{Pr} \simeq 600$), Cholemari and Arakeri [15] ($\mathrm{Pr} \simeq 600$), and the DNS results of Schmidt *et al.* [18] ($\mathrm{Pr} = 1$). The scaling $\mathrm{Nu}_g \sim (\mathrm{Ra}_g\mathrm{Pr})^{\frac{1}{2}}$ is observed in all the cases distinctly. In the DNS results of Schmidt *et al.* [18] at $\mathrm{Ra}_g\mathrm{Pr} \simeq 1.6 \times 10^5$, a departure can be noted which seems like the transition in the scaling as in the case of experiments using heat. A similar transition seems also to be present in the results of experiments using brine [16] at $\mathrm{Ra}_g\mathrm{Pr} \simeq 5.6 \times 10^{10}$. Thus the transition from $(\mathrm{Ra}_g\mathrm{Pr})^{\frac{1}{2}}$ regime is observed for $\mathrm{Pr} = 1$, $\mathrm{Pr} \simeq 6$, and $\mathrm{Pr} \simeq 600$ but at different Rayleigh numbers. It turns out that the flux data including the transition can be consolidated into a single curve by dividing the flux relations by Pr. Variation of $\mathrm{Nu}_g/\mathrm{Pr}$ with Gr_g is shown in Fig. 6, for the results from different studies consolidated in Fig. 5. The transition for all the three Pr values of 1, 6, and 600 occurs at a single value of Gr_g, $\mathrm{Gr}_{gc} \simeq 1.6 \times 10^5$, and the available data for $\mathrm{Pr} = 1$ and $\mathrm{Pr} \simeq 600$ seem consistent with $\mathrm{Gr}_g^{0.3}$ scaling below this critical value. The flux scalings for the two regimes are thus

$$\mathrm{Nu}/\mathrm{Pr} = (0.75 \pm 0.1)\mathrm{Gr}_g^{\frac{1}{2}}, \quad \mathrm{Gr}_g > 1.6 \times 10^5, \tag{4}$$

$$\mathrm{Nu}/\mathrm{Pr} = (8.3 \pm 3)\mathrm{Gr}_g^{0.3}, \quad \mathrm{Gr}_{g1} < \mathrm{Gr}_g < 1.6 \times 10^5. \tag{5}$$

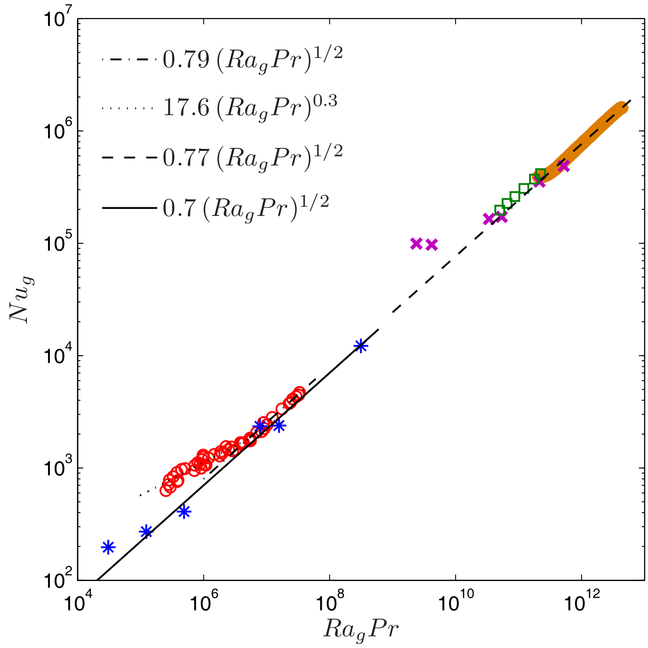

FIG. 5. Nu_g vs $Ra_g Pr$ obtained from various studies: filled circles (orange online) from brine experiments, $Pr \simeq 600$; hollow circles (red online) from heat experiments, $Pr \simeq 6$; hollow squares (green online) from Cholemari and Arakeri [15], $Pr \simeq 600$; crosses (magenta online) from Tovar [16], $Pr \simeq 600$; and stars (blue online) from Schmidt *et al.* [18], $Pr = 1$.

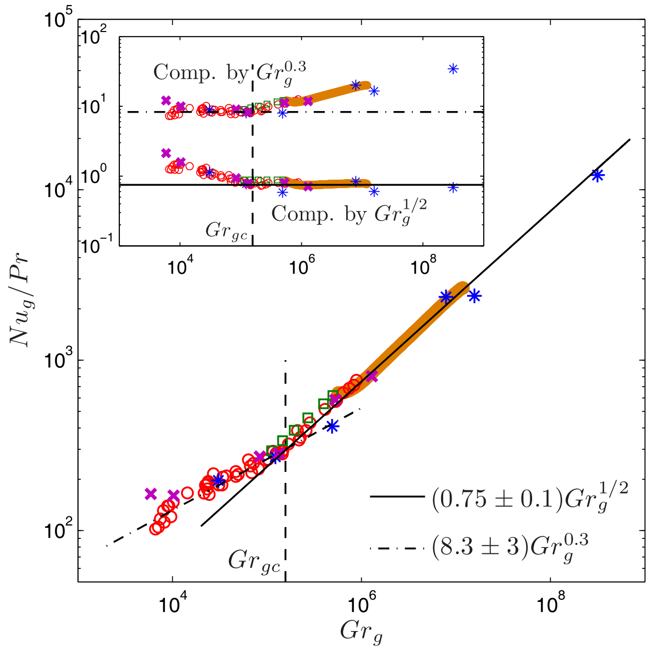

FIG. 6. Variation of Nu_g/Pr with Gr_g in different studies. The symbols are the same as those shown in Fig. 5. Inset shows the data compensated by $Gr_g^{0.3}$ and $Gr_g^{1/2}$.

The latter scaling implies that the flux is no longer independent of viscosity. We may expect another transition to another regime below Gr_{g1}, whose value is not known now. Also, for low Pr, there have been no studies and the Gr_{gc} value as well as the scaling are expected to be different.

To understand the transition between the two regimes and the collapse using the Grashof number, we note that the velocity fluctuations in the vertical direction are affected by viscosity near the wall (Fig. 3 inset). Length scale for the viscosity-dominated region near the wall may be estimated as $l_v \sim \sqrt{\nu\tau}$, where τ is eddy turnover time $= d/w_m$. Thus, $l_v = c_1 d \mathrm{Gr}_g^{-1/4}$, where c_1 is a constant. $\mathrm{Gr}_{gc} = 1.6 \times 10^5$ gives $l_v = 0.05\, c_1 d$. For $l_v/d < 0.05\, c_1$ therefore it seems that the viscosity does not significantly affect the flux transport and $\frac{1}{2}$ power law is observed. Available data from the experiments using brine (velocity profiles shown in Fig. 3) and from Schmidt *et al.* [18] show that the peak in the vertical velocity fluctuations shifts away from the wall and the viscous layer grows with reducing Grashof number. If l_v is taken as the location of the peak from the wall, then from the experimental data, $c_1 \simeq 2.8$, thus giving $l_v \simeq 0.15d$ at Gr_{gc}.

We note that Riedinger *et al.* [22] also report the transitions in the flux scalings in an inclined channel. With increasing inclination angle, successively they obtain a hard turbulence regime with $\mathrm{Nu} \sim (\mathrm{RaPr})^{1/2}$, a soft turbulence regime with $\mathrm{Nu} \sim (\mathrm{RaPr})^2$, an intermediate regime of $\mathrm{Nu} \sim (\mathrm{RaPr})$, and a laminar regime in which $\mathrm{Nu} \sim (\mathrm{RaPr})^{1/4}$ is obtained. The transitions obtained by them and the one in the present case are probably different since the flow in the inclined channel has mixed effects of unstable stratification (in the axial direction) and stable stratification (in the direction perpendicular to the channel axis) [23]. Also unlike in the present case, the mean flow and the Reynolds shear stresses are nonzero in the inclined channel flow. We, however, cannot conclude from the flux data alone whether the change from $1/2$ to 0.3 scaling corresponds to transition from hard turbulence to soft turbulence.

In summary, at sufficiently high Rayleigh number we observe $\mathrm{Nu}_g \sim (\mathrm{Ra}_g\mathrm{Pr})^{1/2}$ in both brine ($\mathrm{Pr} \simeq 600$) and heat ($\mathrm{Pr} \simeq 6$) experiments. Below a certain Ra_g value, a different scaling $\mathrm{Nu}_g \sim (\mathrm{Ra}_g\mathrm{Pr})^{0.3}$ is seen in the heat experiments, which is similar to the one commonly observed in turbulent RBC. However, the Pr dependence of Nu in the two cases is very different. It may also be noted that although the scaling exponents are similar, as mentioned above, the flux transport and the scaling exponent $n \simeq 0.3$ in RBC is essentially due to and explained by the boundary layer dynamics. We do not have an explanation for the exponent $n = 0.3$ in the present flow. This type of transition is also found to be present but at different values of Ra_g in the data reported for $\mathrm{Pr} = 1$ [18] and $\mathrm{Pr} \simeq 600$ [16]. However, we find that the transition occurs at a single Grashof number value of $\mathrm{Gr}_{gc} \simeq 1.6 \times 10^5$ and the fluxes in the two regimes may be given by $\mathrm{Nu}_g/\mathrm{Pr} \sim \mathrm{Gr}_g^{1/2}$ and $\mathrm{Nu}_g/\mathrm{Pr} \sim \mathrm{Gr}_g^{0.3}$, for the three Pr values. Reynolds number scaling $\mathrm{Re} \sim \mathrm{Ra}_g^{1/2}\mathrm{Pr}^{-1/2}$ is also obtained from the measurements in brine experiments. Finally, we note that the fluxes and the Reynolds numbers in tube convection are much larger than those obtained in RBC at the same Rayleigh numbers. For example, for $\mathrm{Ra}_g = 7.58 \times 10^9$ and $\mathrm{Pr} = 600$, the Nusselt number is larger by about four orders of magnitude and the Reynolds number is larger by about two orders of magnitude than those obtained in RBC [24,25] for the same values of Ra and Pr. Similarly the heat flux for $\mathrm{Ra}_g = 2.98 \times 10^5$ and $\mathrm{Pr} = 6$ in tube convection is larger by about three orders of magnitude than the corresponding heat flux in RBC [26]. The two flows are fundamentally different, and the absence of horizontal walls and the associated boundary layers makes the fluxes and Reynolds numbers much higher in tube convection.

[1] G. Ahlers, S. Grossmann, and D. Lohse, Heat transfer and large scale dynamics in turbulent Rayleigh-Benard convection, Rev. Mod. Phys. **81**, 503 (2009).

[2] S. A. Theerthan and J. H. Arakeri, A model for near wall dynamics in turbulent Rayleigh-Benard convection, J. Fluid Mech. **373**, 221 (1998).

[3] B. A. Puthenveettil and J. H. Arakeri, Plume structure in high Rayleigh number convection, J. Fluid Mech. **542**, 217 (2005).

[4] R. Kraichnan, Turbulent thermal convection at arbitrary prandtl number, Phys. Fluids **5**, 1374 (1962).

[5] E. A. Spiegel, Convection in stars I: Basic Boussinesq convection, Annu. Rev. Astron. Astrophys. **9**, 323 (1971).

[6] S. Grossmann and D. Lohse, Scaling in thermal convection: A unifying theory, J. Fluid Mech. **407**, 27 (2000).

[7] J. J. Niemela, L. Skrbek, K. R. Sreenivasan, and R. J. Donnelly, Turbulent convection at very high Rayleigh numbers, Nature (London) **404**, 837 (2000).

[8] P. E. Roche, F. Gauthier, R. Kaiser, and J. Salort, On the triggering of the ultimate regime of convection, New J. Phys. **12**, 085014 (2010).

[9] X. He, D. Funfschilling, H. Nobach, E. Bodenschatz, and G. Ahlers, Transition to the Ultimate State of Turbulent Rayleigh-Benard Convection, Phys. Rev. Lett. **108**, 024502 (2012).

[10] P. Urban, P. Hanzelka, T. Kralik, V. Musilova, A. Srnka, and L. Skrbek, Effect of Boundary Layers Asymmetry on Heat Transfer Efficiency in Turbulent Rayleigh-Bénard Convection at Very High Rayleigh Numbers, Phys. Rev. Lett. **109**, 154301 (2012).

[11] S. Grossmann and D. Lohse, Multiple scaling in the ultimate regime of thermal convection, Phys. Fluids **23**, 045108 (2011).

[12] X. Chavanne, F. Chilla, B. Castaing, B. Hebral, B. Chabaud, and J. Chaussy, Observation of the Ultimate Regime in Rayleigh-Benard Convection, Phys. Rev. Lett. **79**, 3648 (1997).

[13] J. H. Arakeri, F. E. Avila, J. M. Dada, and R. O. Tovar, Convection in a long vertical tube due to unstable stratification—a new type of turbulent flow? Curr. Sci. **79**, 859 (2000).

[14] M. R. Cholemari and J. H. Arakeri, Experiments and a model of turbulent exchange flow in a vertical pipe, Int. J. Heat Mass Transf. **48**, 4467 (2005).

[15] M. R. Cholemari and J. H. Arakeri, Axially homogeneous, zero mean flow buoyancy-driven turbulence in a vertical pipe, J. Fluid Mech. **621**, 69 (2009).

[16] R. O. Tovar, Estudios sobre transicion y turbulencia en flujos de conveccion natural, Ph.D. thesis, Centro de Investigacion en Energia, Universidad Nacional Autonoma de Mexico, Mexico, D.F., 2002 (unpublished).

[17] M. Gibert, H. Pabiou, F. Chilla, and B. Castaing, High Rayleigh Number Convection in a Vertical Channel, Phys. Rev. Lett. **96**, 084501 (2006).

[18] L. E. Schmidt, E. Calzavarini, D. Lohse, F. Toschi, and R. Verzicco, Axially homogeneous Rayleigh-Benard convection in a cylindrical cell, J. Fluid Mech. **691**, 52 (2012).

[19] D. Lohse and F. Toschi, Ultimate State of Thermal Convection, Phys. Rev. Lett. **90**, 034502 (2003).

[20] E. S. C. Ching and T. C. Ko, Ultimate-state scaling in a shell model for homogeneous turbulent convection, Phys. Rev. E **78**, 036309 (2008).

[21] M. Gibert, H. Pabiou, J. C. Tisserand, B. Gertjerenken, B. Castaing, and F. Chilla, Heat convection in a vertical channel: Plumes versus turbulent diffusion, Phys. Fluids **21**, 035109 (2009).

[22] X. Riedinger, J. C. Tisserand, F. Seychelles, B. Castaing, and F. Chilla, Turbulent transport regimes in an inclined channel, Phys. Fluids **25**, 015117 (2013).

[23] Y. Hallez and J. Magnaudet, Buoyancy-induced turbulence in a tilted pipe, J. Fluid Mech. **762**, 435 (2015).

[24] K. Q. Xia, S. Lam, and S. Q. Zhou, Heat Flux Measurement in High Prandtl Number Turbulent Rayleigh-Benard Convection, Phys. Rev. Lett. **88**, 064501 (2002).

[25] S. Lam, X. D. Shang, S. Q. Zhou, and K. Q. Xia, Prandtl number dependence of the viscous boundary layer and the Reynolds numbers in Rayleigh-Benard convection, Phys. Rev. E **65**, 066306 (2002).

[26] T. Y. Chu and R. J. Goldstein, Turbulent convection in a horizontal layer of water, J. Fluid Mech. **60**, 141 (1973).